(Received 26 April 2024, Accepted 22 July 2024, Scheduled 14 August 2024)

High Sensitivity Biosensor Photonic Crystal Focused on Detecting the Concentration of the Biological Analytes

Mohamed A. Ghezal[1, *], Hamza Lidjici[2], Abdelhalim Zoukel[1], Asma Benchiheb[3], and Abdesselam Hocini[4]

[1] *Laboratoire Physico-Chimie des Matériaux, Université de Laghouat, Laghouat, Algérie*
[2] *Laboratoire des Matériaux Pour Applications et Valorisation des Énergies Renouvelables Université de Laghouat, Laghouat, Algérie*
[3] *Laboratoire des Microsystemes et Instrumentation, Universite Constantine 1, Constantine, Algérie*
[4] *Laboratoire d'Analyse des Signaux et Systemes, Deparetement d'Electronique Universite Mohamed Boudiaf de M'sila, BP. 166, Route Ichebilia, M'sila 28000, Algérie*

ABSTRACT: The performance and response characteristics of simulated optical biosensor have been greatly enhanced in this work. The results were obtained by evaluating three different structures, each varying in the number of holes surrounding the cavity. The guide-cavity coupling's structural and dimensional characteristics were varied for an effective comparative study. The high sensitivity quality of this optical biosensor was achieved using large transmission rate. The results showed sensitivity around 800 nm/RIU in the first version, 800 nm/RIU in the second version, and 700 nm/RIU in the last version. Furthermore, the design parameters were optimized by finite difference time domain (FDTD) method.

1. INTRODUCTION

Photonic Band Gap materials or photonic crystals are structures whose dielectric constant is periodically modulated. These materials have frequency bands for which the propagation of electromagnetic waves is prohibited. Like electrons in semiconductors, photons are distributed in transmission bands separated by forbidden bands (band gaps), and this analogy makes it possible to envisage the use of photonic crystals as basic materials for the production of components for integrated optics.

In recent years, the term "photonic crystals" has gained extensive recognition and undergone rapid development [1, 2]. This periodic structure possesses distinctive electromagnetic properties attributed to the presence of a Photonic Band Gap (PBG) [3, 4]. Currently, photonic crystals are widely employed in various applications, showcasing remarkable optical properties, including a photon band gap and the "slow photon" effect, making them particularly valuable in solar cell design [5]. Additionally, these crystals find widespread use in the design of waveguides, sensors [6, 7], reflectors [8], filters [9], and other devices. The unique structure, architecture, and shape of these devices allow very precise control over the light flow [10].

Optical sensors play a pivotal role in promptly detecting and quantitatively measuring biological analyses and diagnostics, holding significant importance and promise. Their multifaceted properties, such as safety in flammable materials and explosive environments, immunity to electromagnetic interference, superior performance, fast response, and capabilities in remote sensing, enhance their appeal. Furthermore, these materials exhibit the ability to concentrate light within a small volume, facilitating substantial interaction with the optical material. This phenomenon renders the sensor highly sensitive to even minor changes in the refractive index (RI) induced by biological species adhering around the pores of the Photonic Crystal (PhC) [11].

The sensing technique must be optimal, selective, and sensitive in proportion to the concentration of the biological solutions. Currently, different techniques for settings and configurations are constantly being developed and improved to increase detection performance and effectiveness.

Therefore, choosing the appropriate biosensor design is a crucial task that must be handled with precision and care to obtain reliable and accurate sensing. Various configurations and designs of biosensors have been proposed, modified, and implemented using different types of PhC structures such as small cavities [12, 13], resonators [14], waveguides [15, 16], hole arrays [17, 18], and heterostructures [19]. All of them exploit resonance conditions that are highly sensitive to directed modes in PhC with respect to RI changes in the medium. Research is constantly evolving to better discover our health disorders by using modern, sophisticated and accurate devices. All of this is aimed at the precise detection of diseases, their details, and the study of their regular and irregular components by conducting a set of biochemical examinations and tests.

Photonic crystals, characterized by high density, exhibit extraordinary sensitivity and selectivity, coupled with real-time monitoring capabilities. This compelling combination has progressively motivated researchers to broaden the scope and ap-

* Corresponding author: Mohamed Aboutaleb Ghezal (ghezal.aboutaleb@gmail.com).

plication areas of these crystals, particularly within the realms of medicine and biochemistry. The periodic formation of these materials is a crucial aspect that enables the creation of a photonic band gap, marking a pivotal feature [20]. This distinctive characteristic has been crucial in identifying cancer cells [21].

In this paper, our primary goal is to develop and enhance the capabilities of the sensor, particularly for detecting diseases in the human body. We aim to achieve higher sensitivity and accuracy than previous designs.

2. DESCRIPTION OF THE STRUCTURE

In our study, Figure 1(a) elegantly illustrates the 2D photonic crystal (PhC) in the x-z plane, featuring a meticulously crafted two-dimensional hexagonal lattice with dimensions of 40×23. This intricate structure comprises a silicon (Si) slab with a refractive index of $n_{si} = 3.48$, on which air holes have been engraved. The air holes, each with a radius of $r = 0.3 \times a$, where 'a' represents the lattice constant ($a = 0.35$ µm), contribute to the overall design of the photonic crystal. After making several modifications to the period, we finalized it, with the value $a = 0.35$ µm representing the maximum length of the range.

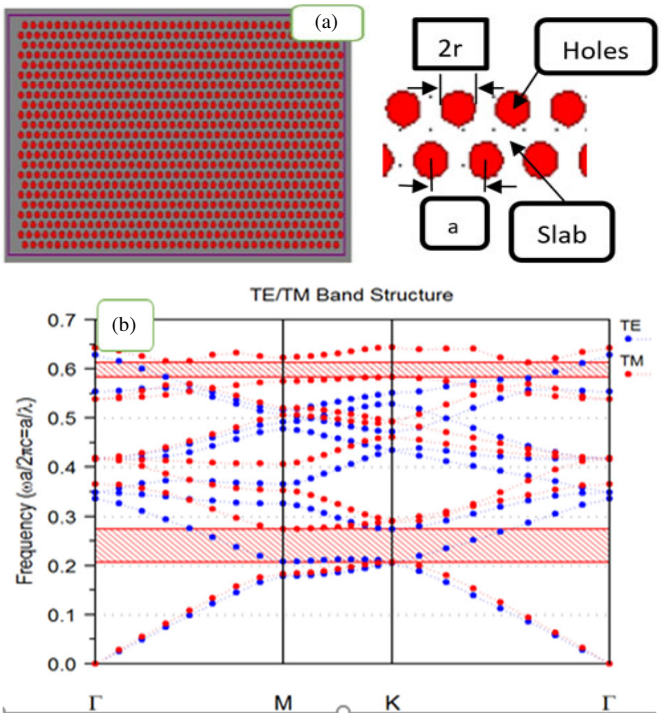

FIGURE 1. (a) Schematic structure of 2D PhC formed by triangular network. (b) Dispersion diagram and band gap for the TM polarization of the structure based on of air holes patterned in silicon (Si) slab ($n_{si} = 3.48$), $a = 0.35$ µm with $r = 0.3 \times a$.

One of the paramount characteristics of this photonic crystal is its band gap, a crucial factor in its optical properties. The band diagram, initially calculated for the PhC structure with circular air holes and devoid of defects, delineates the Edge Γ-M-K-Γ path within the Brillouin zone. The precise calculation is facilitated by the Plane Wave Expansion (PWE) method of the Band Solve software. The plane wave expansion method [22, 23] stands out as the prevalent technique for computing the PBG. In this method, the electromagnetic field is systematically expanded through plane waves, and the magnetic field/electric field along with the dielectric constant is determined through the superposition of these plane waves, employing Fourier transform and Bloch theorem. Subsequently, the solutions to Maxwell's equations [24] are derived through this process.

In our numerical simulations, we adopted a comprehensive approach, utilizing the effective index method [25]. This approach amalgamates both the 2D Plane Wave Expansion (2D PWE) and the 2D Finite Difference Time Domain (2D FDTD) methods, both seamlessly accessible through the RSoft software.

The results of our study, as depicted in Figure 1(b) showcase a pronounced wide band forbidden region centered around a normalized frequency (a/λ) of 0.2395. This distinctive band predominantly appearing in the TM mode is evident, occupying the normalized frequencies of $0.274(a/\lambda)$ to $0.205(a/\lambda)$. These frequencies correspond to a wavelength range from 1.277 µm to 1.707 µm, underscoring the significant optical characteristics of the studied photonic crystal.

3. NUMERICAL SIMULATION AND ANALYSIS

Figure 2(a) provides a clear representation of the refractive index profile through a contour map of the hole and slab, incorpo-

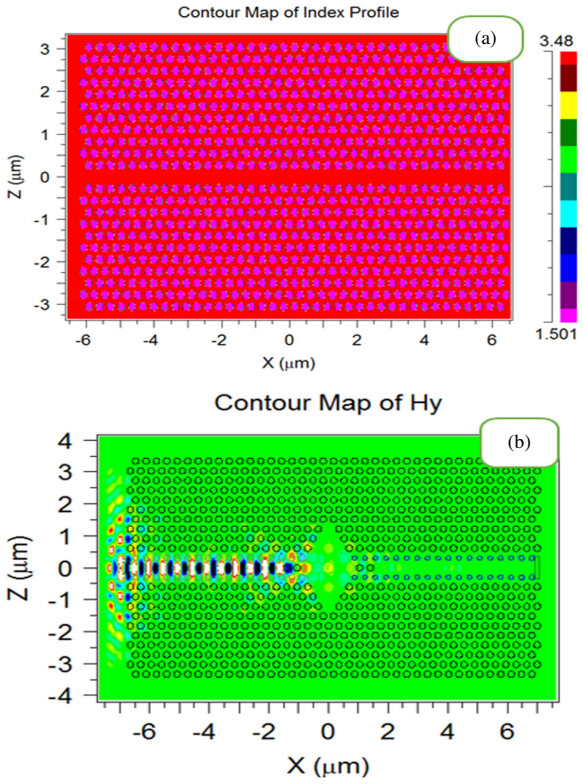

FIGURE 2. (a) Contour map of the refractive index profile of the hole and slab with a linear waveguide along the x-axis (the color bar indicates the refractive index ranging from 1.501 to 3.48). (b) Distribution of the electric field through the guide $W1$ and the structure of the cavity in the x-z plane.

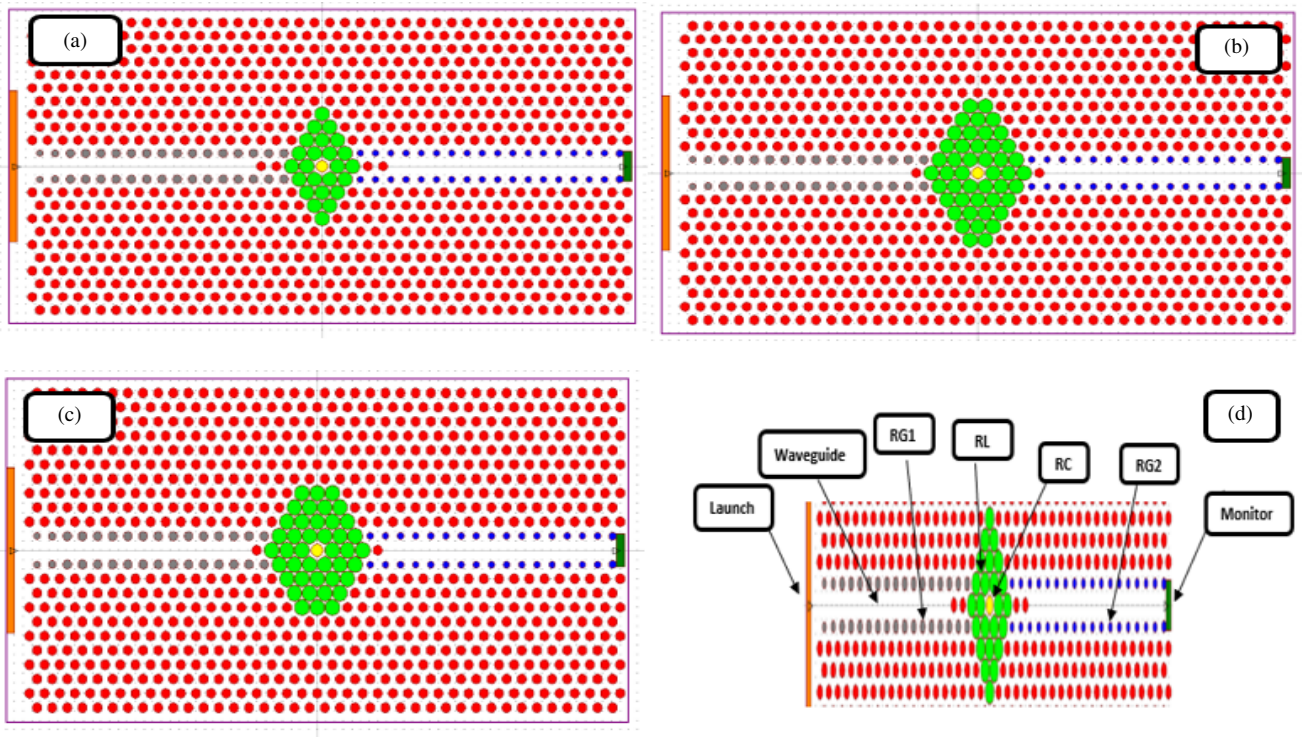

FIGURE 3. Schematic diagram of the biosensor structure indicating the number of functionalized holes around the resonant cavity. (a) 25 holes, (b) 47 holes and (c) 43 holes. (d) Detail of the structure.

rating a linear waveguide along the x-z plane. The accompanying color bar facilitates an easy interpretation of the refractive index values, spanning from 1.501 to 3.48. In Figure 2(b), a detailed illustration is presented, showcasing the electric field distribution along the guide W_1. Additionally, the structure of the cavity is revealed in the x-z plane, offering a comprehensive view of the electromagnetic characteristics within the designed system.

The schematic provides a side-sectional view of the biosensor under design. The device comprises two waveguide couplers and a singular cavity. The formation of the two waveguides involves the removal of a single row of air holes in the x-direction. These waveguides serve the purpose of facilitating the coupling of light into and out of the photonic crystal (PhC) cavity [26]. It is commonly understood that the periodicity of the dielectric function of a PhC is disrupted when defects are introduced into its regular lattice structure. Consequently, the waveguide W_1 is created by excluding a row of air holes in the photonic lattice in the ΓK direction [27].

In the context of this research, we relied on existing studies and data related to the structure of the cavity, its dimensions, and the number of holes surrounding it. It is worth noting that Hocini et al. previously achieved a sensitivity of 588.77 nm/RIU, as shown in Figure 3(d) [32]. Hence, we used their findings as a basic reference point, with the aim of enhancing sensitivity in our work. The highest sensitivity values of 609.25 nm/RIU, 737 nm/RIU, 720 nm/RIU, and 496 nm/RIU were obtained by Tayoub et al. [28], Rahman-Zadeh et al. [29], Danaie and Kiani [30] and Zaky et al. [31], respectively. The results were obtained for total infiltration, where all the air holes around the cavity are infiltrated. However, based on these results and their conclusions, we have assigned $RC = 0.39 \times a$ and $RL = 0.49 \times a$. We have proposed three different shapes for the gap in terms of the number of holes: 25, 47, and 43, and we proposed new and ideal dimensions for the radius of all the holes in the edge of the carrier $w1$, as shown in the picture in two colors, $RG1 = 0.9 \times r$ and $RG2 = 0.7 \times r$, to improve the performance and sensitivity of the sensor and reach better and larger values than before.

In our study, we examined a variety of solutions with their own refractive index, namely benzene ($n = 1,501$), cedar oil ($n = 1,516$), ethyl salicylate ($n = 1,523$), chlorobenzene ($n = 1,525$), and methyl salicylate ($n = 1,538$). The investigation focused on the impact of altering the number of the holes surrounding the cavity, on both the output ratio and sensor sensitivity. The obtained results reveal distinct trends based on the number of modulated holes. Notably, configurations in Figure 3(a) with 25 holes and Figure 3(b) with 47 holes demonstrated superior sensitivity performance, reaching up to 800 nm/RIU. The output ratio consistently remained around 1, and the wavelength closely matched the telecom wavelength of 1550 nm. Meanwhile, Figure 3(c) achieves a sensitivity of 700 nm/RIU, which is remarkably high and comparable to the rates observed in the preceding figures. We have created the two figures below to facilitate careful analysis of the results obtained. In Figure 4(a), the presentation of the ideal resonance wavelength serves to enhance our understanding of the wavelength that is most conducive to achieving optimal sensor performance. The resonance wavelength refers to the specific wavelength at which the sensor's sensitivity and respon-

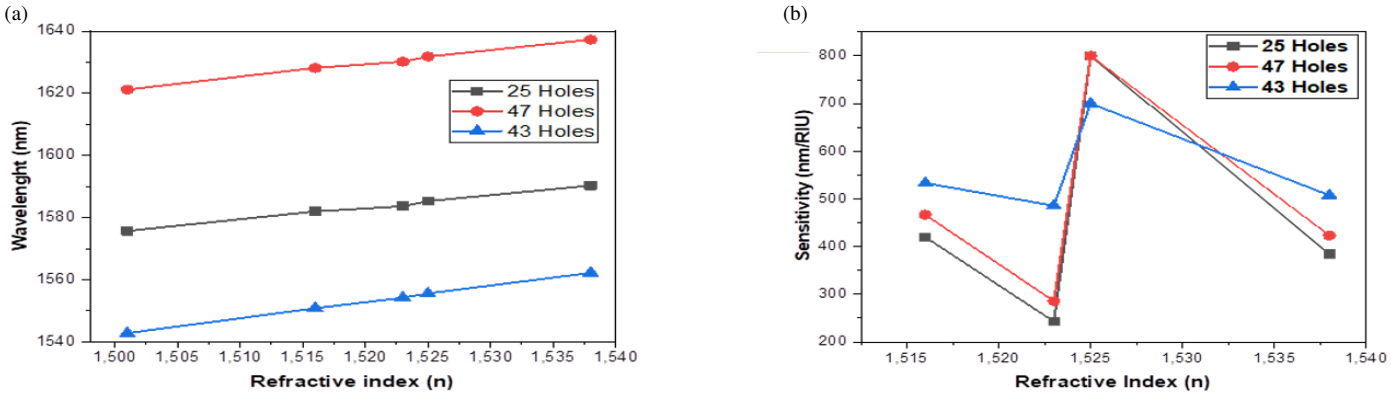

FIGURE 4. (a) Variation of wavelength as function of refractive index. (b) Variation of sensitivity as function of refractive index.

TABLE 1. Sensitivity of the biosensor 25 holes for different liquid.

Réfractive index (n_1)	Réfractive index (n_2)	λ_1 (nm)	λ_2 (nm)	Sensitivity (nm/RIU)
$n = 1.501$	$n = 1.516$	1575.7	1582	420
$n = 1.516$	$n = 1.523$	1582	1583.7	242.85
$n = 1.523$	$n = 1.525$	1583.7	1585.3	800
$n = 1.525$	$n = 1.538$	1585.3	1590.3	384.61

TABLE 2. Sensitivity of the biosensor 47 holes for different liquid.

Réfractive index (n_1)	Réfractive index (n_2)	λ_1 (nm)	λ_2 (nm)	Sensitivity (nm/RIU)
$n = 1.501$	$n = 1.516$	1621.2	1628.2	466.66
$n = 1.516$	$n = 1.523$	1628.2	1630.2	285.71
$n = 1.523$	$n = 1.525$	1630.2	1631.8	800
$n = 1.525$	$n = 1.538$	1631.8	1637.3	423.07

TABLE 3. Sensitivity of the biosensor 43 holes for different liquid.

Réfractive index (n_1)	Réfractive index (n_2)	λ_1 (nm)	λ_2 (nm)	Sensitivity (nm/RIU)
$n = 1.501$	$n = 1.516$	1542.8	1550.8	533.33
$n = 1.516$	$n = 1.523$	1550.8	1554.2	485.71
$n = 1.523$	$n = 1.525$	1554.2	1555.6	700
$n = 1.525$	$n = 1.538$	1555.6	1562.2	507.69

siveness are maximized. By identifying this wavelength, researchers can fine-tune the sensor's design and operation to ensure that it operates efficiently and effectively within desired parameters. Overall, Figure 4(a) not only presents the resonance wavelength but also aims to elucidate its significance in achieving peak sensor performance. This understanding is crucial for advancing sensor technology in various fields such as spectroscopy, biomedical diagnostics, and environmental monitoring.

Figure 4(b) meticulously explores the influence of three distinct sensor shapes on contrast sensitivity, particularly in response to varying refractive indices of chemical solutions. This analysis not only deepens our comprehension of sensor performance but also directly guides the refinement of sensor designs for applications demanding precise optical detection capabilities. This analysis plays a pivotal role in advancing sensor technology by guiding the design of more effective sensors capable of precise optical detection across a wide range of applications. The pictures were created based on the results presented in Tables 1, 2, and 3, respectively.

Figure 5 illustrates the output spectrum of a proposed sensor under varying configurations of modulated holes surrounding the cavity, (a) 25 holes, (b) 47 holes, and (c) 43 holes. These results highlight the significant influence of adjusting both the

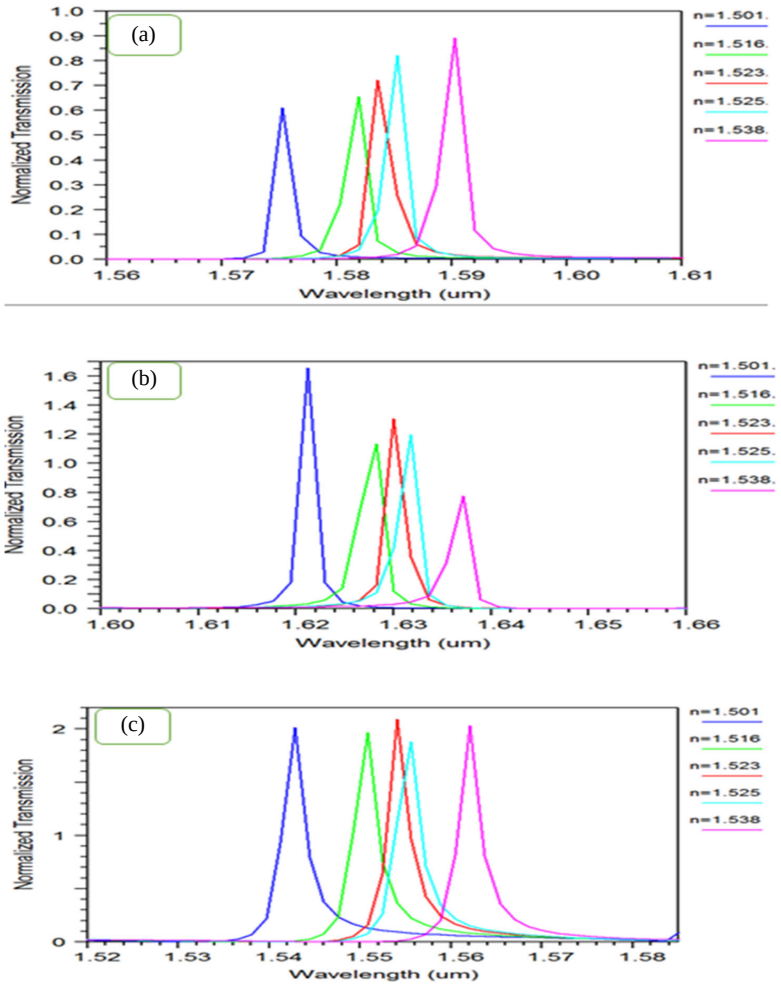

FIGURE 5. The transmission spectrum of the proposed sensor for a different number of modulated holes around the cavity. (a) 25 holes, (b) 47 holes and (c) 43 holes.

diameter and number of holes on sensor performance, with particular emphasis on achieving optimal sensitivity with configurations employing 25 and 47 holes. This analysis underscores the importance of meticulous design optimization to achieve optimal sensitivity and enhance the overall effectiveness of optical sensors in practical applications. Table 4 was created to compare our work with previous similar studies.

TABLE 4. Comparison of the proposed biosensor with various similar PhC designs.

References	Sensitivity (nm/RIU)
[28]	609.25
[29]	737
[31]	496
[30]	720
[11]	462.61
In this work	
Design A	800
Design B	800
Design C	700

4. CONCLUSIONS

This study has focused on the design and characterization of three different biosensors with varying numbers of holes around the cavities. The objective was to investigate the impact of the number of holes on the sensitivity of the biosensors. Through extensive simulation and analysis, the obtained results clearly demonstrate the significant effect of the number of holes on biosensor sensitivity.

By applying different solutions and calculating the wavelength of transmission for each solution, we were able to quantify and compare the sensitivity of the biosensors. The findings revealed a strong correlation between the number of holes and the sensitivity of the biosensors, with an increase in the number of holes leading to higher sensitivity.

These results underscore the significant potential of these biosensors for a multitude of applications that demand high sensitivity. The capability to fine-tune and optimize sensitivity by adjusting the number of holes offers a promising strategy for customizing biosensor performance to meet specific requirements.

Additionally, this study highlights the successful development of biosensors that exhibit both high sensitivity and robust

performance. The precise detection and measurement capabilities of these biosensors demonstrate their applicability in diverse fields such as medical diagnostics, environmental monitoring, and food safety.

This research not only enhances the understanding of biosensor technology but also underscores the critical importance of optimizing design parameters, such as the number of holes, to improve sensitivity. The achieved results pave the way for further advancements and broader applications in the field of biosensing, setting a foundation for future research in this dynamic and rapidly evolving area. The insights gained from this study open new avenues for developing highly sensitive biosensors tailored to specific needs, thereby expanding their utility across various scientific and industrial domains.

REFERENCES

[1] Yablonovitch, E., "Inhibited spontaneous emission in solid-state physics and electronics," *Physical Review Letters*, Vol. 58, No. 20, 2059, 1987.

[2] John, S., "Strong localization of photons in certain disordered dielectric superlattices," *Physical Review Letters*, Vol. 58, No. 23, 2486, 1987.

[3] Wang, Y., S. Chen, P. Wen, S. Liu, and S. Zhong, "Omnidirectional absorption properties of a terahertz one-dimensional ternary magnetized plasma photonic crystal based on a tunable structure," *Results in Physics*, Vol. 18, 103298, 2020.

[4] Yablonovitch, E., T. J. Gmitter, and K.-M. Leung, "Photonic band structure: The face-centered-cubic case employing nonspherical atoms," *Physical Review Letters*, Vol. 67, No. 17, 2295, 1991.

[5] Liu, W., H. Ma, and A. Walsh, "Advance in photonic crystal solar cells," *Renewable and Sustainable Energy Reviews*, Vol. 116, 109436, 2019.

[6] Goban, A., C.-L. Hung, J. D. Hood, S.-P. Yu, J. A. Muniz, O. Painter, and H. J. Kimble, "Superradiance for atoms trapped along a photonic crystal waveguide," *Physical Review Letters*, Vol. 115, No. 6, 063601, 2015.

[7] Young, A. B., A. C. T. Thijssen, D. M. Beggs, P. Androvitsaneas, L. Kuipers, J. G. Rarity, S. Hughes, and R. Oulton, "Polarization engineering in photonic crystal waveguides for spin-photon entanglers," *Physical Review Letters*, Vol. 115, No. 15, 153901, 2015.

[8] Kumar, A., N. Kumar, and K. B. Thapa, "Tunable broadband reflector and narrowband filter of a dielectric and magnetized cold plasma photonic crystal," *The European Physical Journal Plus*, Vol. 133, No. 7, 250, 2018.

[9] Awasthi, S. K., R. Panda, and L. Shiveshwari, "Multichannel tunable filter properties of 1D magnetized ternary plasma photonic crystal in the presence of evanescent wave," *Physics of Plasmas*, Vol. 24, No. 7, 072111, 2017.

[10] Aly, A. H., S. A. El-Naggar, and H. A. Elsayed, "Tunability of two dimensional n-doped semiconductor photonic crystals based on the Faraday effect," *Optics Express*, Vol. 23, No. 11, 15 038–15 046, 2015.

[11] Arafa, S., M. Bouchemat, T. Bouchemat, A. Benmerkhi, and A. Hocini, "Infiltrated photonic crystal cavity as a highly sensitive platform for glucose concentration detection," *Optics Communications*, Vol. 384, 93–100, 2017.

[12] Hocini, A., R. Moukhtari, D. Khedrouche, A. Kahlouche, and M. Zamani, "Magneto-photonic crystal microcavities based on magnetic nanoparticles embedded in silica matrix," *Optics Communications*, Vol. 384, 111–117, 2017.

[13] Hocini, A. and A. Harhouz, "Modeling and analysis of the temperature sensitivity in two-dimensional photonic crystal microcavity," *Journal of Nanophotonics*, Vol. 10, No. 1, 016007, 2016.

[14] Hsiao, F.-L. and C. Lee, "Computational study of photonic crystals nano-ring resonator for biochemical sensing," *IEEE Sensors Journal*, Vol. 10, No. 7, 1185–1191, 2010.

[15] Skivesen, N., A. Têtu, M. Kristensen, J. Kjems, L. H. Frandsen, and P. I. Borel, "Photonic-crystal waveguide biosensor," *Optics Express*, Vol. 15, No. 6, 3169–3176, 2017.

[16] Bougriou, F., T. Bouchemat, M. Bouchemat, and N. Paraire, "Optofluidic sensor using two-dimensional photonic crystal waveguides," *The European Physical Journal — Applied Physics*, Vol. 62, No. 1, 11201, 2013.

[17] Zhang, Y.-N., Y. Zhao, and Q. Wang, "Multi-component gas sensing based on slotted photonic crystal waveguide with liquid infiltration," *Sensors and Actuators B: Chemical*, Vol. 184, 179–188, 2013.

[18] Lai, W.-C., S. Chakravarty, X. Wang, C. Lin, and R. T. Chen, "On-chip methane sensing by near-IR absorption signatures in a photonic crystal slot waveguide," *Optics Letters*, Vol. 36, No. 6, 984–986, 2011.

[19] Di Falco, A., L. O'Faolain, and T. F. Krauss, "Chemical sensing in slotted photonic crystal heterostructure cavities," *Applied Physics Letters*, Vol. 94, 063503, 2009.

[20] Clark, L., Jr., "Implantable gas-containing biosensor and method for measuring an analyte such as glucose," US patent 4,680,268, 1987.

[21] Hadi, S. and S. Eskandari, "Sensing blood components and cancer cells with photonic crystalresonator biosensor," *Optic*, Vol. 14, 100593, Feb. 2024.

[22] Zabel, I. H. H. and D. Stroud, "Photonic band structures of optically anisotropic periodic arrays," *Physical Review B*, Vol. 48, No. 8, 5004–5012, 1993.

[23] Zouache, T., A. Hocini, and X. Wang, "Cavity-coupled photonic crystal waveguide as highly sensitive platform for pressure sensing," *Optik*, Vol. 172, 97–106, Nov. 2018.

[24] Johnson, S. G. and J. D. Joannopoulos, "Block-iterative frequency-domain methods for Maxwell's equations in a planewave basis," *Optics Express*, Vol. 8, No. 3, 173–190, 2001.

[25] Qiu, M., "Effective index method for heterostructure-slab-waveguide-based two-dimensional photonic crystals," *Applied Physics Letters*, Vol. 81, No. 7, 1163–1165, 2002.

[26] Dutta, H. S., A. K. Goyal, and S. Pal, "Sensitivity enhancement in photonic crystal waveguide platform for refractive index sensing applications," *Journal of Nanophotonics*, Vol. 8, No. 1, 083088, 2014.

[27] Zhao, Y., C. Qian, K. Qiu, Y. Gao, and X. Xu, "Ultrafast optical switching using photonic molecules in photonic crystal waveguides," *Optics Express*, Vol. 23, No. 7, 9211–9220, 2015.

[28] Tayoub, H., A. Hocini, and A. Harhouz, "Design and analysis of a high-performance capsule-shaped 2D-photonic crystal biosensor: Application in biomedicine," *Journal of Nano- and Electronic Physics*, Vol. 13, No. 6, 06005, 2021.

[29] Rahman-Zadeh, F., M. Danaie, and H. Kaatuzian, "Design of a highly sensitive photonic crystal refractive index sensor incorporating ring-shaped GaAs cavity," *Opto-Electronics Review*, Vol. 27, No. 4, 369–377, Dec. 2019.

[30] Danaie, M. and B. Kiani, "Design of a label-free photonic crystal refractive index sensor for biomedical applications," *Photonics and Nanostructures — Fundamentals and Applications*, Vol. 31, 89–98, Sep. 2018.

[31] Zaky, Z. A., M. Al-Dossari, N. Saleh, M. M. Abdelhady, A. Sharma, V. D. Zhaketov, and A. H. Aly, "Photonic crystal with magnified resonant peak for biosensing applications," *Physica Scripta*, Vol. 98, No. 5, 055108, Apr. 2023.

[32] Hocini, A., K. Boudiaf, and H. Safer, "Etude et conception des capteur a cristaux photoniques pour des applications biomedicals," N°: 2018/ESEM 08/87, Tech. Rep., Juin 2018.